Proceedings of ninth International Conference on Hydro-Science and Engineering (ICHE 2010), IIT Madras, Chennai, India.
2 - 5 August 2010

3D NUMERICAL SIMULATION OF SEDIMENT TRANSPORT AROUND SPUR-DIKES UNDER VARIOUS INSTALLATION CONDITIONS

T.Nabatake[1], I.Kimura[2], Y.Shimizu[3] and S.Kawamura[4]

***Abstract**: This paper describes the numerical study on 3D turbulent flow structures and bed deformations around spur-dikes. First, we tested the accuracy of 3D numerical model including bed sediment transport equations by comparison between numerical results and previous experimental results. Effects of two hydraulic parameters, S/L (S:interval length of two spur dikes, L: length of spur dikes) and θ (= inclination angle), are then examined using the present numerical model. The relation of 3D flow features and the bed variations depending on the hydraulic conditions is discussed.*

***Keywords**: 3D CFD model; Open channel flow; Local scour; Spur dikes*

1 INTRODUCTION

Recently, the excellent effects of improving river environment by spur dikes are recognized widely. An embayment formed around Spur-Dikes due to sedimentation, which is called "Wando" in Japan, provides favorable habitat for wide variety of fauna and flora. Figure 1 shows an example of a group of Wando in Kiso River in Japan. The processes of formation of the embayment and the governing hydraulic parameters have not been elucidated enough. Therefore, it is necessary to clarify the time-mean and time-dependent behavior of the 3D flow pattern as well as bed shape deformations around spur dikes.

Fig. 1. Spur dikes and "Wando" in Kiso River

Tominaga et al (2006) performed the laboratory tests using PIV under various hydraulic conditions. Those results have indicated that the inclination angle and the interval of spur dikes are important parameters for 3D flow patterns as well as the bed topography around spur dikes.

1 Research Student, Graduate school of Engineering Hokkaido University ,N13 W8, Kita-ku, Sapporo Hokkaido Japan, Email: double.back-flip@eng.hokudai.ac.jp
2 Professor, Graduate school of Engineering Hokkaido University ,N13 W8, Kita-ku, Sapporo Hokkaido Japan, Email: i-kimu2@ eng.hokudai.ac.jp
3 Professor, Graduate school of Engineering Hokkaido University ,N13 W8, Kita-ku, Sapporo Hokkaido Japan, Email: yasu@ eng.hokudai.ac.jp
4 Professor, Graduate school of Engineering Hokkaido University ,N13 W8, Kita-ku, Sapporo Hokkaido Japan, Email: s-kawamr@ eng.hokudai.ac.jp

In this study, 3D (three dimensional) turbulent flow structures and bed deformations around spur dikes under various hydraulic conditions are examined numerically. First, the accuracy of the present numerical model is tested through the comparison with the experiment results performed by Hinokidani et al (1992). Then, the model is applied to spur dikes under various hydraulic conditions in order to clarify the effects of hydraulic parameters on flows and bed formations. A special attention is given to the influence of two hydraulic parameters: (i) the inclination angle between mainstream and spur dikes, and (ii)S/L (S: interval length of two spur dikes, L: length of spur dikes). Figure 2 shows schematic diagram of flow domain and notations of symbols.

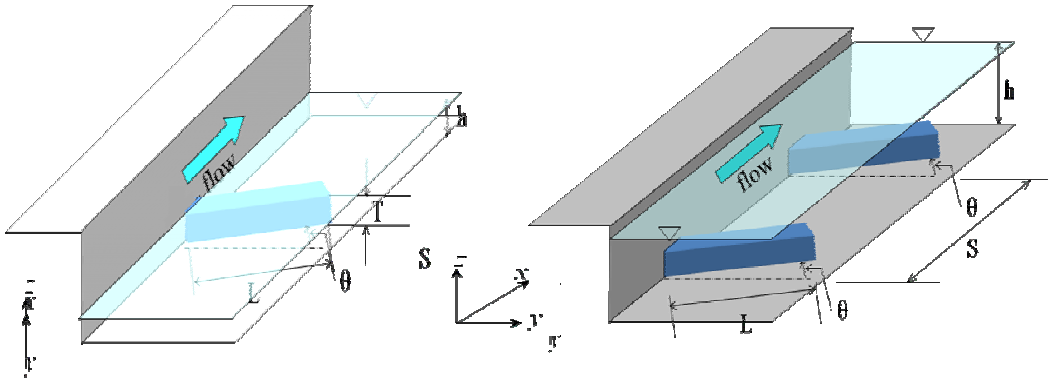

i) Run A (focusing on inclined angle) **ii) Run B (focusing on S/L spur dikes interval)**

Fig 2. Schematic diagram of the flow field and notations of symbols

2 COMPUTATIONAL METHOD

2.1 Basic Equations

The Reynolds averaged 3D flow equations with contravariant components of velocity vectors on a generalized curvilinear movable coordinate system are used as governing equations for computations. The equations are composed of a continuity equation, momentum equations and k-ε equations as follows.

[Continuity equation]

$$\frac{1}{\sqrt{g}}\frac{\partial V^{\alpha}\sqrt{g}}{\partial \xi^{\alpha}} = 0 \tag{1}$$

[Momentum equation]

$$\frac{\partial V^{i}}{\partial t} + \nabla_j[V^i(V^j - W^j)] + V^i\nabla_j W^j + V^j\nabla_j W^i = F^i - \frac{1}{\rho}g^{ij}\nabla_j p + \nabla_j[-\overline{v^i v^j}] + 2\nu\nabla_j e^{ij} \tag{2}$$

[k equations]

$$\frac{\partial k}{\partial t} + \nabla_j[k(V^j - W^j)] + k\nabla_j W^j = -g_{ij}\overline{v^i v^j}\nabla_j V^i - \varepsilon + \left\{\left(\frac{D_t}{\sigma_k} + \nu\right)g^{ij}\nabla_i k\right\} \tag{3}$$

[ε equations]

$$\frac{\partial \varepsilon}{\partial t} + \nabla_j[\varepsilon(V^j - W^j)] + \varepsilon\nabla_j W^j = -C_{\varepsilon 1}\frac{\varepsilon}{k}g_{ij}\overline{v^i v^j}\nabla_j V^i - C_{\varepsilon 2}\frac{\varepsilon^2}{k} + \nabla_j\left\{\left(\frac{D_t}{\sigma_k} + \nu\right)g^{ij}\nabla_i \varepsilon\right\} \tag{4}$$

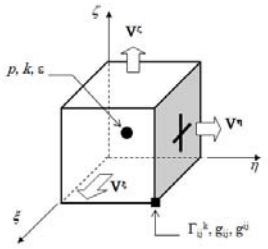

Fig 3. Arrangement of hydraulic variables and metric tensors on full staggered grid

where ξ^I= generalized curvilinear coordinate (see Figures 2 and 3), t= time, V^i= contravariant component of the velocity vector of flows, W^i= contravariant component of the velocity vector of grid motion, p= pressure, ν= molecular dynamic viscosity, ρ= density of water, k= turbulent energy, ε= turbulent energy dissipation rate, g_{ij} and g^{ij}=covariant and contravariant component of metric tensor, g= det(g_{ij}), and F^i= contravariant component of gravity acceleration. ∇^I indicates a covariant differential, for inst*ance,*

$$\nabla_i A^k = \frac{\partial A^k}{\partial \xi^i} + A^j \Gamma_{ij}^{\ k} \tag{5}$$

where $\Gamma_{ij}^{\ k}$= Christoffel symbol described as

$$\Gamma_{ij}^{\ k} = \begin{Bmatrix} k \\ ij \end{Bmatrix} = \frac{1}{2} g^{km} \left(\frac{\partial g_{jm}}{\partial \xi^i} + \frac{\partial g_{im}}{\partial \xi^j} - \frac{\partial g_{ij}}{\partial \xi^m} \right) = \frac{\partial \xi^k}{\partial x^p} \frac{\partial^2 x^p}{\partial \xi^i \xi^j} \tag{6}$$

To calculate a complex turbulent flow with separation and vortex shedding, a 2nd-order non-linear k-ε model by Kimura & Hosoda (2003) is adopted as a turbulence model. This model has been applied to various flow fields, such as, a flow around a surface-mounted cubic obstacle (Kimura & Hosoda 2000) and a compound open channel flow (Kimura et al 2001). The constitutive equations of the model are described as follows.

$$-\overline{v'^i v'^j} = D_t S^{ij} - \frac{2}{3} k \delta_s^i g^{sj} - \frac{k}{\varepsilon} D_t [\alpha_1 Q_1 + \alpha_2 Q_2 + \alpha_3 Q_3] \tag{7}$$

$$D_t = C_\mu \frac{k^2}{\varepsilon} \tag{8}$$

$$Q_1 = S^{i\alpha} g_{\alpha l} \Omega^{lj} + S^{j\beta} g_{\beta l} \Omega^{li} \tag{9}$$

$$Q_2 = S^{i\alpha} g_{\alpha} \Omega^{lj} - \frac{1}{3} S^{k\alpha} g_{\alpha m} S^{m\beta} g_{\beta k} \delta_l^i g^{lj} \tag{10}$$

$$Q_3 = \Omega^{i\alpha} g_{\alpha l} \Omega^{lj} - \frac{1}{3} \Omega^{k\alpha} g_{\alpha m} \Omega^{m\beta} g_{\beta k} \delta_l^i g^{ij} \tag{11}$$

$$S^{ij} = g^{j\alpha} \nabla_\alpha V^i + g^{i\alpha} \nabla_\alpha V^j \tag{12}$$

$$\Omega^{ij} = g^{j\alpha} \nabla_\alpha V^i - g^{i\alpha} \nabla_\alpha V^j \tag{13}$$

The model coefficients are not constants but functions of the strain parameter S and the rotation parameter Ω. In this study, all the coefficients are given as functions with one variable M for simplicity as follows (Ali et al. 2007).

$$\alpha_1 = -0.1325 f_M, \quad \alpha_2 = 0.0675 f_M, \quad \alpha_3 = -0.0675 f_M \tag{14}$$

$$f_M = \frac{1}{1+0.02M^2}, \quad M = \max[S,\Omega] \tag{15}$$

$$C_\mu = \min[0.09, \frac{0.3}{1+0.09M^2}] \tag{16}$$

$$S = \frac{k}{\varepsilon}\sqrt{\frac{1}{2}S^{i\alpha}g_{\alpha j}S^{j\beta}g_{\beta i}} \tag{17}$$

$$\Omega = \frac{k}{\varepsilon}\sqrt{\frac{1}{2}\Omega^{i\alpha}g_{\alpha j}\Omega^{j\beta}g_{\beta i}} \tag{18}$$

2.2 Bed load model

We employed the Kovacs and Parker's equation for calculation of bed load transport in the stream-wise direction and Hasegawa's equation for the sediment transport in the lateral direction of stream line. Those equations are shown as:

[Streamline direction]

$$q_{BS} = \frac{K}{\left(1+\frac{\partial z_b}{\partial x}\Big/\mu_c\right)}\left[\tau^* - \tau_c^*\left(1+\frac{\partial z_b}{\partial x}\Big/\mu_c\right)\right]\times\left[\tau^{*1/2} - \tau_c^{*1/2}\left(1+\frac{\partial z_b}{\partial x}\Big/\mu_c\right)^{1/2}\right] \tag{19}$$

[Lateral direction of stream line]

$$q_{Bn} = q_{BS}\left(-\frac{\partial z_b}{\partial n}\sqrt{\frac{\tau_c^*}{\mu_s\mu_k\tau^*}}\right) \tag{20}$$

The change of bed height by the sediment transport was computed using the following bed continuity equation in the generalized curvilinear form.

[Continuity equation of river-bed]

$$\frac{\partial}{\partial t}\left(\frac{z_b}{J}\right) + \frac{1}{1-\lambda}\left(\frac{\partial}{\partial\xi}\left(\frac{q_B^\xi}{J}\right) + \frac{\partial}{\partial\eta}\left(\frac{q_B^\eta}{J}\right)\right) = 0 \tag{21}$$

2.3 Outline of numerical method

The differential equations governing the mean-velocities and the turbulence field are solved with the finite volume method on full-staggered grid system. The arrangement of hydraulic variables on a full-staggered grid is shown in Figure 2. The metric tensors and the Cristoffel symbols are defined only at grid points to save computational memory and the values at other positions are interpolated at each computational step.

The QUICK scheme is applied to the convection terms and the central differencing is used for the diffusion terms in the momentum equations. The hydrid central upwind scheme is applied to the k and ε equations for the computational stability. The Adams-Bashforth scheme with second-order accuracy in time is used for time integration in each equation. The basic equations are discretized as fully explicit forms and are solved successively along the time axis step by step.

The pressure field is solved using iterative procedure at each time step using SOLA algorithm by Hirt et al. (1975).

2.4 Boundary conditions

Since the present turbulence model is a high Reynolds number type, the wall function approach is applied as the wall boundary conditions for k and ε. The wall friction is evaluated by the log-law. At the downstream end of the computational domain, the longitudinal gradients of all variables are assumed to be zero. At the boundary inlet, the level of k is chosen to be $(0.02U_0)^2$ (U_0= bulk velocity).

The free surface elevation is solved by the simple relation in Equation (22) since the contravariant components of the velocity vector are used in the basic equations (Takizawa et al. 1992).

$$\Delta h = \sqrt{g_{33}} V^3 \Delta t \tag{22}$$

where Δt= time increment and Δh= surface elevation during Δt. To consider the rapid attenuation of turbulent intensities in the depth-wise direction near the free surface, the eddy viscosity is multiplied by the following dumping function (Hosoda 1990).

$$f_s = 1 - \exp(-B\frac{(h-y)\varepsilon_s}{k_s^{3/2}}), \text{ (B=10)} \tag{23}$$

where sub-s indicates the value at the surface layer. The turbulent dissipation rate ε at the surface layer is evaluated by the following formula proposed by Sugiyama et al (1995) to calculate the secondary currents of 2nd kind.

$$\varepsilon_s = \frac{C_{\mu 0}^{3/4} k_s^{3/2}}{0.4\Delta y_s}, \ (C_{\mu 0}=0.09) \tag{24}$$

2.5 Initial conditions

At the beginning of the calculation, U (= velocity in the longitudinal direction (ξ-direction)) = U_0 (= averaged bulk velocity), V (= velocity in the transverse direction (η-direction) = 0, k = k_{in} and ε = ε_{in} (k_{in} and ε_{in} are the values of k and ε at the inlet boundary) are specified over the whole computational domain. The initial bed form is assumed as flat. In order to avoid the influence of the initial conditions, the numerical results after 50 seconds from the initial conditions are used for the following analysis.

3 COMPUTATIONAL CONDITHIONS

Spur dikes are constructed in a group in usual river works. However, we consider a flow field, in which only two spur dikes with same length, height, angle, etc. are attached to the left bank, for simplicity. The following two hydraulic parameters are considered.

i) Case A. θ: inclination angle between a spur dike and lateral direction of the main stream
ii) Case B. S/L : S = spatial interval of two spur dikes and L = length of a spur dike

4. RESULTS AND DISCUSSIONS

4.1 Calibration of the computational model (Case A)

The accuracy of the prediction of 3D flow pattern around spur dikes has already been checked by Kimura et al (2003). The accuracy of the computations of bed variations is examined in the present study using the experimental data provided by Hinokidani et al

(1992). The hydraulic parameters and the computational grid are shown in Table 1 and Figure 4, respectively. Figure 6 shows the contour of bed variations at t=200 (sec). It is thought that the present computational result could capture well the scouring area around a spur dike and sedimentation area behind a spur dike. The deposition height behind a spur dike is also predicted sufficiently. However, predicted maximum scour depth is about 2cm shallower than the experiment result. Those results indicate that the present model has sufficient performance to investigate the bed topography around spur dikes.

Table 1 Hydraulic conditions for Case A

Run	θ	Direction of inclination	Common parameters
A1	-30	Upstream inclined	B=40cm, L=10cm
A2	0	Right angled	h_l=4cm, h=2.85cm, Q=4l/s
A3	30	Downstream inclined	D_0=0.06cm Slope=1/300

h_l=height of Spur dikes , h= height of water, D_0=Diameter of sand

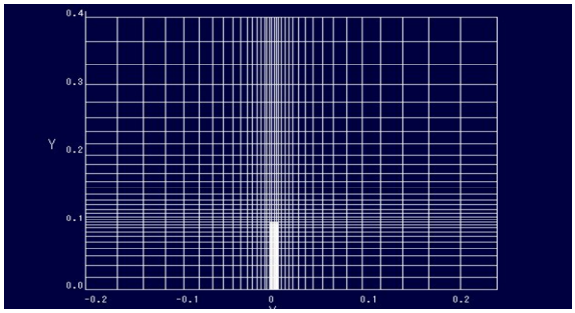

Fig 4 Computational grid for Case A.

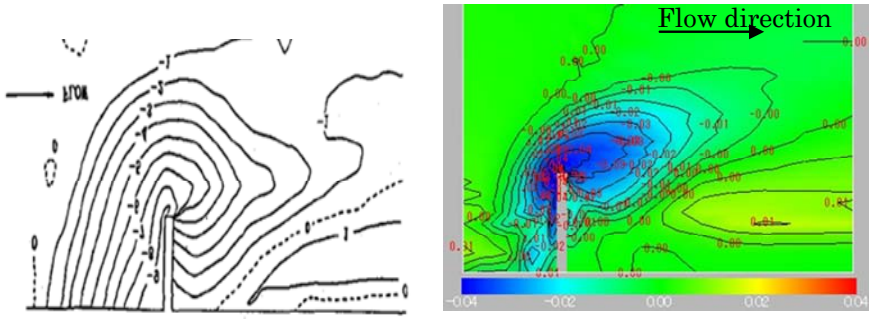

a) Experimental result **b) Numerical result**

Fig 6 Comparison of experimental and numerical results (Case A2)

4.2 Effect on inclination angle

In case A2 and A3, the scouring area is larger than that in A1. The results in A2 and A3 show the flow from root to tip along front of spur dikes. The flow seems to enlarge the scoring area. The flow of A2 that is showed red circle is strong, this is reason that A2 scouring area is broader than A3 that. In case A1 sedimentation area can be seen at upstream region of a spur dike. This difference seems to be caused by the flow toward upstream of sedimentation area from a spur dike root. In all cases, sedimentation area of downstream of a

spur dike is not different. In downstream of a spur dike the flow direction is same, but strength of flow and vortex behind a spur dike are different.

Table 2 Hydraulic condition

Run	S/L	Common parameters
B1	2	B=30cm, L=5cm
B2	3	h_l=4cm, h=8cm, Q=8.2l/s
B3	4	D_0=0.04cm Slope=1/2000

h_l=height of spur dikes , h= depth of water, D_0=diameter of sand

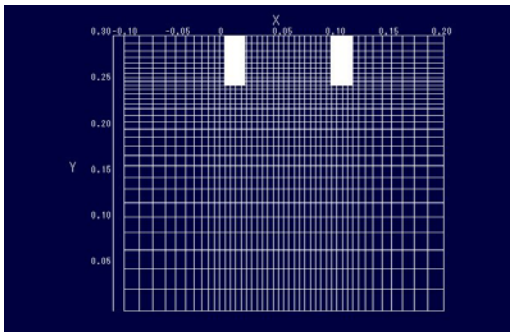

Fig 6 Computational grid for Case B

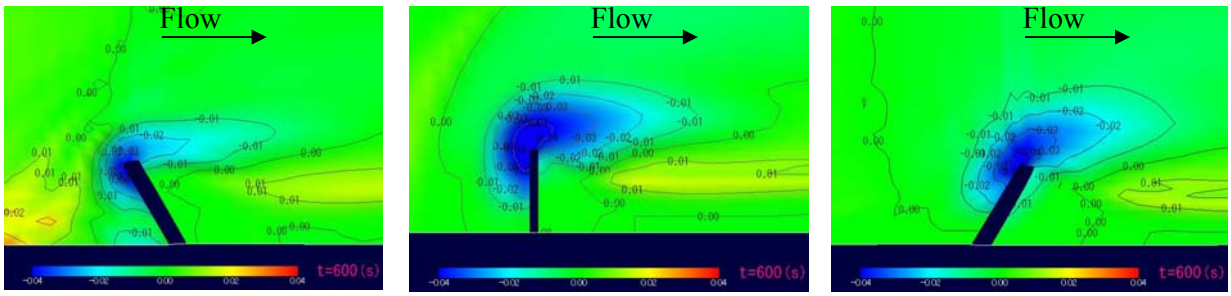

A1) Upstream inclined **A2) Right** **A3) Downstream inclined**

Fig 7 Numerical results of Case A (contour of bed variations)

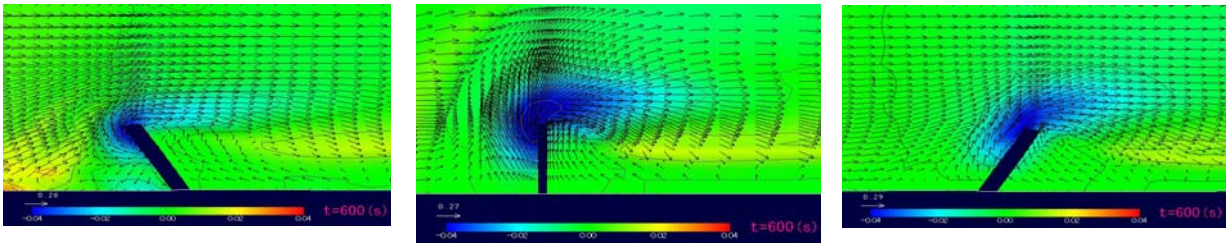

A1) Upstream inclined **A2) Right angle** **A3) Downstream inclined**

Fig 8 Numerical results of Case A (vector around a spur dike (z= 5mm))

4.3 Effect on interval of spur dikes (Case B)

Figure 9 and 10 show the comparison of bed configuration and velocity vectors in Cases B1-B3. In case B3, deposition and scour are generated outside of the spur dikes area. This reason is horizontal vortex between spur dikes become extended to downstream direction, and the flow strength is weaker than other case. In case B1, sedimentation height becomes the highest. Sedimentation area between two spur dikes locates same location in case B1 and B2, and sedimentation area is 7cm upstream of 2nd spur dike. In case B1, it is thought that sedimentation height become high because the 1st spur dike capture the sand. Next, we would like to consider the scouring area around 2nd spur dikes. In case B1, the scouring area is extended to the front of the 2nd spur dike, on the other hand, in case B2, a scouring area can be seen from the tip of the spur dikes to the downstream direction. In case B1, the flow is generated along the front of spur dike, but in case B2 the flow is generated from tip to downstream direction. So, we can understand that the flow direction is closely related to scoring and sedimentation area.

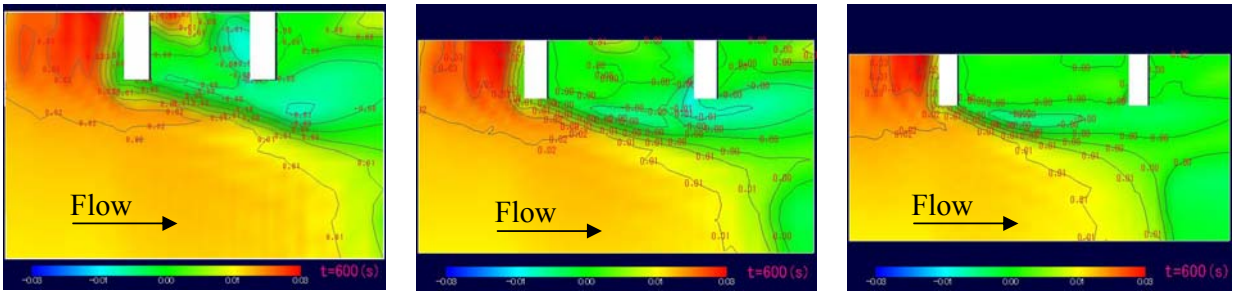

B1) 2times interval **B2) 3times interval** **B3) 4times interval**

Fig 9 Color contour of bed fluctuation

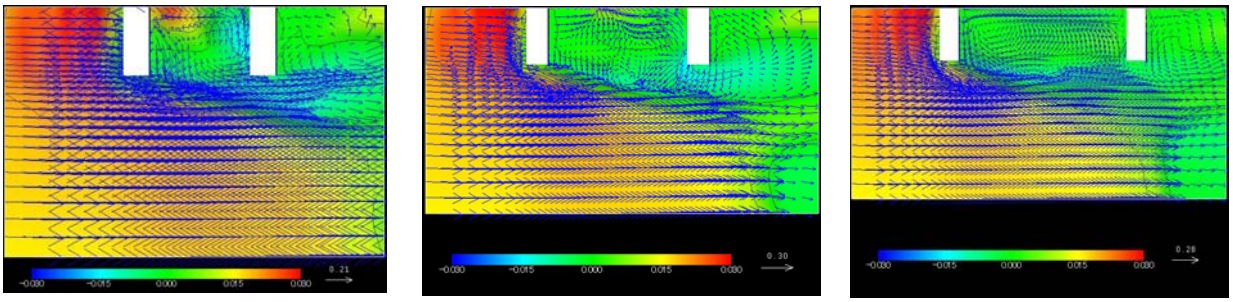

B1) 2times interval **B2) 3times interval** **B3) 4times interval**

Fig 10 vector around a spur dike (z= 5mm)

Figure 11 shows temporal variations of velocities in the transverse direction (y-direction) between the tips of two spur dikes at z =40mm. This figure shows that the flow in case B1 is steady and the flows in other 2 yield fluid oscillation. The amplitude of the oscillation is about 4cm/s and the period is 0.7s in case B2. In case B3, the amplitude is 0.3cm/s and the period is 3 (s). We checked the Strouhal number defined as

$$S_t = \frac{fS}{U_0}$$

where f= frequency of fluid oscillation, S= interval length of two obstacle and U_0= bulk

velocity. The Strouhal number becomes St=0.62 in case B2. (Nakamura and Nakashima (1986)) showed that the Strouhal number of the fluid oscillation around a steel bar with H-type cross section becomes around 0.6. The present result is in good agreement with the result by Nakamura and Nakashima (1986).

Table 3 shows the bed variations between two spur dikes. These results show that if the spur dikes interval is longer, difference of bed variation becomes smaller. Sedimentation volume is largest in Case B3 and smallest in B2. Therefore, we can understand that the unsteady fluid oscillation has a role to suppress the excessive deposition at the spur dikes zone.

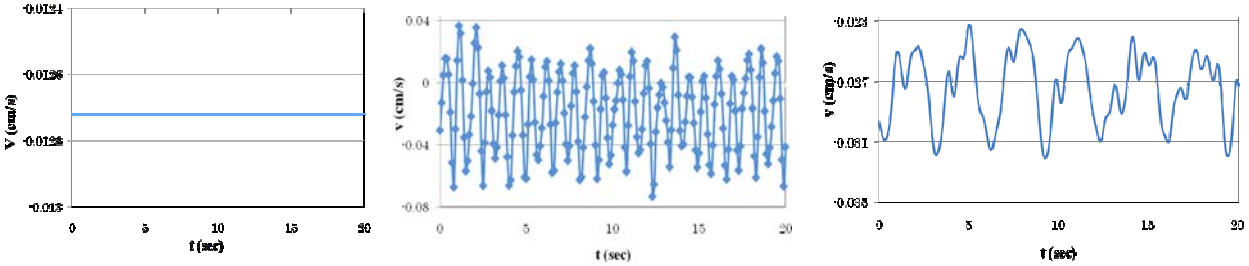

Case B1 **Case B2** **Case B3**

Fig. 11 temporal variations of velocities in the transverse direction

Table 3 bed fluctuation volume

	B1	B2	B3
average sedimentation height (cm)	0.04	0.02	0.07
maximum sedimentation hight(cm)	2.64	1.16	0.43
maximum scoring depth(cm)	-1.26	-1.17	-0.3

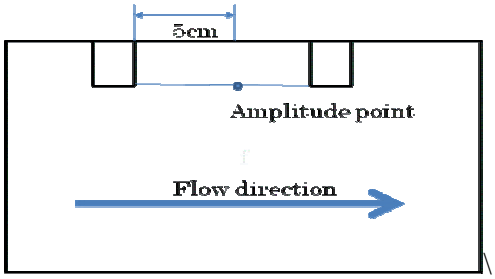

Figure 12 Amplitude point

CONCLUSION

We proposed a 3D numerical model to predict the flow and the bed deformation around spur dikes, and the bed configuration around spur dikes under various hydraulic conditions are investigated numerically. We considered two hydraulic parameters, i) the inclination angle, ii) the interval of two spur dikes. The major findings of our study are listed as follows.

1. The present 3D model could precisely predict the local scour depth around a spur dike.
2. It is shown that the bed topography around a spur dike is closely affected by inclination angle.
3. Numerical result indicated that the magnitude of the fluid oscillation around two spur dikes depends on their interval. The fluid oscillation has a role to suppress the deposition at the spur dikes zone.

REFERENCES

Bosch, G. & Rodi, W., 1998. Simulation of vortex shedding past a square cylinder with different turbulence models. International Journal for Numerical Methods in Fluids, 28:601-616

Chiba, S. & Tkemoto, Y., 1999. A Study of numerical flow simulators of the Ise Bay, the second report –Development of a computer program for generation of two dimensional structural grids, making use of graphical user interface-Yokkaichi University Journal of Environmental and Information sciences, 2(2):103-126(in Japanese).

Gatski, T.B. & Speziale, C.G., 1993. On explicit algebraic stress models for complex turbulent flows. Los Alamos Scientific Report, LA-5852.

Michiue, M. & Hinokidani, O., 1992, Calculation of 2-dimensional bed evolution around spur-dike. Annual Journal of Hydraulic Engineering, JSCE, 36, 61-66 (in Japanese).

Nakamura, Y. & Nakashima, M., 1986, Vortex excitation of prisms with elongated rectangular, H and ├ cross-sections. Journal of Fluid Mechanics, Vol.163, pp.149-169

Hosoda, T., 1990, Ph.D. Thesis, Kyoto University (in Jnapanese).

Hosoda, T., Kimura, I. & Onda, S., 2001. Some necessary conditions for a non-linear k-ε model in classified flow Patterns with a singular point. Proceedings of 2nd International Symposium on Turbulence and Shear Flow Phenomena, Stockholm, Sweden, 3:155-160.

Hosoda, T., Sakurai, T., Kimura, I. &Muramoto, Y.,200.3-D computations of compound open channel flows with horizontal vortices and secondary currents by means of non-linear k-ε model. Journal of Hydroscience and Hydraulic Engineering, 17(2):87-96.

Kawaguchi, H. & Fukuoka, S., 2000. Study on hydrodynamic forces on submersible groins in series. Proceedings of Hydro Informatics, Non-linear Analysis-2, Iowa City, IA, USA(CD-ROM).

Kimura, I., Kitamura, T., Sumi, T., Takeda, M., Onitsuka, K., Sho, K. & Otsuka, K., 2002. Corporative research on morphological evolution and environmental functions of embayed topography formed around spur dikes in the tidal area of the Kiso River. Advances in river Engineering, JSCE, Vol.8, 365-370 (in Japanese).

Kimura, I.. & Hosoda, T., 1999. 3-D unsteady flow structures around rectangular column in open channels by means of non-linear k-ε model. Proceedings of 1st International Symposium on Turbulence and Shear Flow Phenomena, Santa Barbara, CA, USA, 1001-1006.

Kimura, I. & Hosoda, T., 2000. Numerical simulation of flows around a surface-mounted cube by means of a non-linear k-ε model. Proceedings of 9th. International Symposium on Flow Visualization, Edinburgh, Scotland, Paper No.388(CD-ROM).

Kimura, I. & Hosoda, T., 2003. A non-linear k-ε model with realizability for prediction of flows around bluff bodies. International Journal for Numerical Methods in Fluids, 42, Wiley, 813-837.

Kimura, I., Hosoda, T. & Onda, S., 2002a. Numerical simulation full staggered boundary fitted coordinate system for the analysis of 3D turbulent flows in open channels. Yokkaichi University Journal of Environmental and Information Schiences, 4(1): 145-170 (in Japanese).

Kimura, I., Hosoda, T. & Onda, S., 2002b. Prediction of 3D flow structures around skewed spur dikes by means of a non-linear k-ε model. In D. Bousmar and .Y. Zech(eds), River flow 2002, 1:65-73. Rotterdam: Balkema.

Kimura, I., Hosoda, T., Onda, S. & Tominaga, A. 2003. 3D numerical analysis of unsteady flow structures around inclined spur dikes by means of a non-linear k-ε model. Proceeding of the International Symposium on Shallow Flows, Delft, The Netherlands, Part III, 205-212.

Pope, S. B. 1975. A more general effective viscosity hypothesis. Journal of Fluid Mechanics, 72: 331-340.

Rockwell, D. & Naudascher, E., 1978. Review – Self-sustaining oscillations of flow past cavities. Transaction of the ASME, Journal of Fluid Engineering, 100:152-165.

Sugiyama, H., Akiyama, M. & Matsubara, T., 1995. Numerical simulation of compound open channel flow on turbulence with a Reynolds stress model. journal of Hydraulic, Coastal and Environmental Engineering, 515/ II-31:55-65 (in Japanese).

Takizawa, A., Koshizuka, S. & Kondo, S., 1992. Generalization of physical component boundary fitted co-ordinate (PCBFC) method for the analysis of free-surface flow. International Journal for Numerical Methods in Fluids, 15:1213-1237.

Tamoto, N., Tominaga, A. & Ijima, K., 2003. Flow structures in continuous spur dike zone with orientation angle. Proceedings of the 30th Congress of IAHR, Greece, pp.1-6 (CD-ROM).

Tominaga, A., Ijima, K. & Nakao, Y., 2001. PIV analysis of flow structures around skewed spur dikes. Annual Journal of Hydraulic Engineering, JSCE, 45: 379-384 (in Japanese).

Tominaga, A. & Ijima, K., 2002. Effects of interval length on flow structures around submerged spur dikes. Annual Journal of Hydraulic Engineering, JSCE,46, 475-480 (in Japanese).

Weitbrecht, V. & jirka, H., 2001. flow patterns in dead zones of rivers and their effect on exchange processes. Proceeding of 3rd International Symposium on Environmental Hydraulics, Tempe, AZ, USA, (CD-ROM).

Yamashita, Y. Ito, A., Takeda, M. & Matsuo, N. 2001. Proceedings of Annual Conference of Civil Engineers, Chubu Chapter, JSCE, 237-238 (in Japanese).